JACS
JOURNAL OF THE AMERICAN CHEMICAL SOCIETY
pubs.acs.org/JACS
Article

Resolving the Structural Debate for the Hydrated Excess Proton in Water

Paul B. Calio,[†] Chenghan Li,[†] and Gregory A. Voth*

Cite This: J. Am. Chem. Soc. 2021, 143, 18672−18683
Read Online
ACCESS | Metrics & More | Article Recommendations | Supporting Information

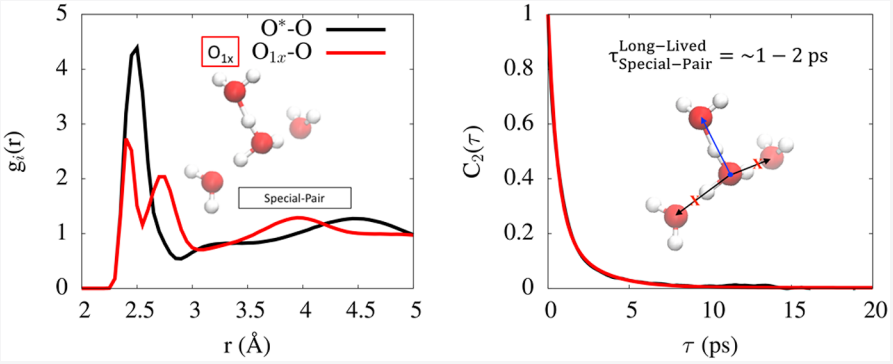

ABSTRACT: It has long been proposed that the hydrated excess proton in water (aka the solvated "hydronium" cation) likely has two limiting forms, that of the Eigen cation ($H_9O_4^+$) and that of the Zundel cation ($H_5O_2^+$). There has been debate over which of these two is the more dominant species and/or whether intermediate (or "distorted") structures between these two limits are the more realistic representation. Spectroscopy experiments have recently provided further results regarding the excess proton. These experiments show that the hydrated proton has an anisotropy reorientation time scale on the order of 1−2 ps. This time scale has been suggested to possibly contradict the picture of the more rapid "special pair dance" phenomenon for the hydrated excess proton, which is a signature of a distorted Eigen cation. The special pair dance was predicted from prior computational studies in which the hydrated central core hydronium structure continually switches (O−H···O)* special pair hydrogen-bond partners with the closest three water molecules, yielding on average a distorted Eigen cation with three equivalent and dynamically exchanging distortions. Through state-of-art simulations it is shown here that anisotropy reorientation time scales of the same magnitude are obtained that also include structural reorientations associated with the special pair dance, leading to a reinterpretation of the experimental results. These results and additional analyses point to a distorted and dynamic Eigen cation as the most prevalent hydrated proton species in aqueous acid solutions of dilute to moderate concentration, as opposed to a stabilized or a distorted (but not "dancing") Zundel cation.

INTRODUCTION

The hydrated excess proton (aka "hydronium cation" plus nearby solvating water molecules) is pervasive in systems relevant to complex problems, e.g., proteins[1−4] and renewable energy materials.[5−7] Characterizing its essential solvation and transport behavior has been an active research area for more than two centuries. In bulk water, the hydrated excess proton has an anomalously high diffusion coefficient in comparison to other +1 cations,[3,8] which is typically described via the Grotthuss mechanism,[9,10] where the net positive charge defect associated with an excess proton translocates over large distances through the breaking and forming of covalent bonds. In addition, the solvation structure of a hydrated excess proton is sometimes described by the limiting cases of either an Eigen cation[11] (a hydronium ion, H_3O^+, core with strong hydrogen bonds to its three surrounding water molecules) or less often as a Zundel cation[12] (an excess proton equally solvated by two flanking water molecules). However, the exact nature of the hydrated excess proton hopping mechanism and most stable solvation structures represents an area of ongoing research interest (see, for example, refs 13 and 14).

The solvation and transport properties of hydrated excess protons have been the topic of numerous simulation studies; see, for example, refs 15−20. The dominant proton transfer (PT) mechanism is believed to be an Eigen−Zundel−Eigen

Received: August 18, 2021
Published: November 1, 2021

(EZE) mechanism, where a "distorted" Eigen cation is the most stable structure and the Zundel cation is mainly an intermediate complex.[21,22] In this vein, proton transport occurs through the cleavage of a hydrogen bond in the second solvation shell, suggesting that Grotthuss hopping occurs via a stepwise process. Although the EZE proton hopping process represents the predominant mechanism, the simulation literature does include suggestions of Zundel−Zundel conversions,[15,18,23,24] although in some of these cases the underlying model appears to introduce a bias toward such a picture.

In actuality, however, the solvation structure of the hydrated excess proton is more complex than either Eigen or Zundel cations. In fact, the hydrated excess proton is seen in a broad range of configurations, making Eigen or Zundel cations only limiting structures and very difficult to deconvolute. For example, Tuckerman et al.[15,25] utilized *ab initio* molecular dynamics (AIMD) simulations of an excess proton in 32 waters to confirm the presence of a "special pair" between the hydronium and nearby water molecules, which is very characteristic of a Zundel cation. Later molecular dynamics (MD) studies characterized the structure of the solvated proton as a distorted Eigen cation, where the 3-fold symmetry is broken due to the distortion of the special pair.[17,22,26] In particular, classical multistate empirical valence bond (MS-EVB) and AIMD simulations were used to confirm that the identity of the special partner is not static, but instead switches with the other two hydrating water molecules in the Eigen cation on time scales of tens of femtoseconds. This "special pair dance" is a process in which the central hydrated hydronium in an Eigen cation ($H_9O_4^+$) structure continually switches special pair partners with its strongly hydrogen-bonded neighboring water molecules on a time scale of tens of femtoseconds.[22] Hence, these studies suggested that the primary structure of the hydrated proton in water is, on average, a "distorted" Eigen cation, but also that this structure is quite dynamic among the three possible special pairs.

Elucidating the solvation structure of the hydrated excess proton is further complicated by the difficulty in correlating experimental infrared frequencies with structural information obtained from MD simulations. Although gas-phase results have been informative in correlating the two,[27−30] the condensed phase introduces further complications due to thermal and quantum fluctuations.[17,31] When compared to the pure water absorption spectrum, four notable features can be seen in the acidic IR spectrum:[32−34] (1) a red shift in the O−H peak of bulk water correlating to stronger hydrogen-bonding environments due to the excess proton; (2) an acid continuum from 2000 to 3200 cm^{-1}, which is most recently ascribed to more distorted Eigen-like configurations;[33] (3) a peak at 1200 cm^{-1} corresponding the proton transfer mode (PTM) between two flanking waters; and (4) a peak at 1750 cm^{-1} corresponding to flanking water bend.

In the past few years, nonlinear spectroscopy experiments have provided pioneering efforts to understand the hydrated excess proton.[35−40] For example, experimental studies of acid clusters in acetonitrile mixtures[36,40] observed the PTM $|1\rangle \rightarrow |2\rangle$ transition was greater than the $|0\rangle \rightarrow |1\rangle$ transition. This result was used to propose a one-dimensional potential energy surface (PES) picture for the PTM that had a symmetric double-well structure, a possible characteristic of a Zundel cation. In water−acid solution,[35] Tokmakoff and co-workers used two-dimensional infrared spectroscopy to excite the O−H stretching vibrations around 3150 cm^{-1} and detected spectral responses within a spectrum ranging from 1500 to 4000 cm^{-1}. By assigning 1760 cm^{-1} to the bending vibration of the flanking waters of the Zundel complex, they suggested that the population of the Zundel cation is larger than previously proposed in theoretical studies. Furthermore, the time scale for the spectral movement from bulk water stretching (3260 cm^{-1}) to proton flanking water bending (1760 cm^{-1}) was shown to be 480 fs, which was interpreted as the lower bound of the Zundel lifetime, leading them to conclude that it may serve as more than a simple PT intermediate. Their subsequent studies[37] using 2D IR further (and importantly to the present topic) suggested that the effective PES is not a symmetric double-energy well characteristic of a symmetric Zundel cation, but rather incorporates a distortion into the underlying PES of the hydrated excess proton (and these authors called it a "distorted Zundel" structure). Additionally, by examining data obtained from parallel and perpendicular 2D IR spectra at 1750 cm^{-1}, two anisotropy time scales of ∼2 ps and ∼200 fs were observed for 2 M HCl solutions,[38] which are both beyond the calculated time scale of the special pair dance.[41] In defining the excess proton as being "Zundel-like" in these studies, these researchers emphasized that the excess proton was shared between two flanking waters, synonymously known as a special pair.

The lower bound of the water-to-proton interconversion time scale (480 fs) determined from 2D-IR spectroscopy[35] was investigated by a computational study using classical and quantum AIMD simulations.[42] These latter authors computed the frequency−frequency correlation function and discovered a 1−2 ps time scale for the 3150 cm^{-1} to 1760 cm^{-1} frequency evolution, consistent with the experimental lower bound. In some ways similar to the approach taken in ref 21, they then utilized a "proton asymmetry coordinate" (ϕ) to decompose the proton spectrum and attributed the 3150 cm^{-1} band to a proton that is less likely to form a strong hydrogen bond with its neighboring water molecule (high-ϕ value) and the 1760 cm^{-1} to a proton that is more likely to form a strong hydrogen bond with its neighboring water molecule (low-ϕ value). Accordingly, the 1−2 ps time scale was attributed to the interconversion between the high-ϕ species to the low-ϕ species, which is a descriptor of water rearrangement in the first and second solvation shell; however, its connection to the Zundel cation lifetime seems unclear. Additionally, that work preceded the most recent nonlinear experiments,[37,38] which presented anisotropy decays.

By using various acid solution trajectories of hydrated excess protons with multiple simulation methods—as well as instantaneous normal-mode analysis—in the present paper we more clearly elucidate the dynamics of the hydrated excess proton, which at the same time also provides a more revealing interpretation of the recent spectroscopic results. In particular, based on these trajectories, we are able to capture specific processes that give rise to the anisotropy decay. As detailed herein, we document the long-lived time scale as corresponding to proton transport observed by recent nonlinear spectroscopy, while confirming the structure of the hydrated excess proton to be best described as a distorted Eigen cation. Additionally, we explore the instantaneous normal modes for the hydrated excess proton that reveal both Eigen and Zundel structures exhibit the 1750 cm^{-1} band.

This paper is outlined as follows: In the next section, we describe the simulation methods used to calculate the data,

https://doi.org/10.1021/jacs.1c08552
J. Am. Chem. Soc. 2021, 143, 18672−18683

while also providing simulation details. This is followed by the Results and Discussion section, where we then use radial distribution functions (RDFs) to show the solvation structure of the hydrated excess proton is best characterized as a distorted Eigen cation. We next provide our anisotropic dynamics data for the distorted Eigen cation, as well as the time evolution of normal modes related to the special pair dynamics. It is noteworthy that we also address the role of nuclear quantum effects in some of the simulations. In the final section, we provide conclusions.

METHODS

Simulation Approaches. Two different and complementary simulation methods were used to carry out this study: the multistate empirical valence bond (MS-EVB) method[43−47] and experiment-directed simulation[48] for *ab initio* molecular Dynamics (EDS-AIMD).[49] We briefly explain the methodology behind these approaches, but we direct the reader to the original literature for further details.

In the MS-EVB formalism, the hydrated excess proton charge defect is dynamically delocalized among multiple water molecules by creating a "wavefunction" that is a linear combination of different bonding topology states. In each diabatic state, a different water molecule is covalently bonded to the excess proton, such that

$$|\Psi\rangle = \sum_{i=1}^{N} c_i |i\rangle \tag{1}$$

Once the linear combination is constructed, the coefficients of the ground state function are determined through an eigenvalue problem using a quantum-like Hamiltonian, as follows:

$$\boldsymbol{Hc} = E_0 \boldsymbol{c} \tag{2}$$

where E_0 and the coefficients are functions of the instantaneous nuclear configuration of the system. In the Hamiltonian the diagonal elements are defined using molecular mechanics force field terms, augmented by a repulsive term to correct for an overattraction of the water molecules to the core hydronium cation. At the same time, the off-diagonal elements are used to couple the different diabatic states and allow transitions between them to occur "on the fly" (and hence to model chemical bonding rearrangements) in the MS-EVB MD simulation.

For this paper, we used the MS-EVB 3.2 and (anharmonic MS-EVB) aMS-EVB 3.2 models.[47] In comparison to earlier MS-EVB models for the excess proton in water,[17,44,45] an additional Lennard-Jones potential energy term is incorporated in the 3.2 version to better account for the fourth water presolvation around the hydronium core.[50] The anharmonic aMS-EVB 3.2 model also incorporates nonharmonic vibrations in solvating the water molecules. In previous work,[34,51,52] the MS-EVB 3.2 model was used to help interpret infrared spectroscopy data of hydrated excess protons in bulk HCl acid and isotopically substituted water solutions. The model also provided cluster configurations extracted from those systems to calculate instantaneous normal modes using electronic density functional theory (DFT) at the B3LYP functional level.

To compare our results with another independent and complementary simulation method, we also utilized EDS-AIMD simulation.[49,53] Such an approach corrects for the overstructuring and slow diffusion of water in BLYP/BLYP-D3-based AIMD simulations by including an additional minimal bias to the system Hamiltonian through a potential energy term (eq 3). In this study, two EDS-AIMD methods are used. The first corrects the system water oxygen−oxygen (Ow−Ow) RDF to better match experiment,[49] hence known as EDS-AIMD(OO), while the second corrects the system water oxygen−hydrogen (Ow−Hw) RDF to match MB-pol's classical water model for this RDF, which is known to be highly accurate.[54−57] This method is known as EDS-AIMD(OH).[53] In either case, the additional EDS potential is given by

$$V(r_i) = \sum_{k=0}^{M} \frac{\alpha_k}{\hat{f}_k} \sum_{j\neq i}^{n_O} r_{ij}^k [1 - u(r_{ij} - r_0)] \tag{3}$$

which is a term added to the DFT potential in the AIMD. It includes the coupling constant (α_k) and the experimental target values ($\hat{f}_k$). This term utilizes a mollified smoothing function to make the coordination number and its statistical moments continuous. The EDS-AIMD(OH) method utilized concepts from Li and Swanson[58] and Li and Voth[59] to bias the hydrogen bond in acidic solutions in a continuous manner, and details are provided in Section S1 of the Supporting Information, denoted later as SI. The coupling constant in eq 3 for EDS-AIMD(OO) was parametrized so that the oxygen−oxygen coordination number and its first through third moments could accurately reproduce experimental results, while the coupling constant for EDS-AIMD(OH) was parametrized to match the oxygen−hydrogen coordination number and its second moment of MB-pol's O−H RDF.[54−57] By directly biasing the coordination number and its moments, other structural and dynamical properties were also seen to be improved without increased AIMD computational cost.[49,53] Most importantly for the present study, the properties of the hydrated excess proton are also significantly improved through the EDS-AIMD approach, including the gas-phase Zundel cation proton transfer barrier, to which the method was not fit, and also the ratio of the excess proton diffusion to water diffusion (see Section S1 of the SI for details).

Simulation Details. In total, 10 independent MS-EVB 3.2 and aMS-EVB 3.2 simulations of 1 HCl in 256 H_2O with a box side length of 19.73 Å were simulated using an in-house version of the LAMMPS simulation package.[60] Water molecules were modeled using SPC/Fw[61] and aSPC/Fw[46] for MS-EVB 3.2 and aMS-EVB 3.2, respectively. A state searching algorithm that selects up to three solvation shells of H_3O^+ was employed to construct the MS-EVB Hamiltonian matrix. After a 1 ns nonreactive equilibration period, each simulation was equilibrated using our reactive molecular dynamics simulation code for 500 ps in the constant NVT ensemble using a Nose-Hoover chain thermostat with chain length of 3 with a temperature set to 298 K and a time constant of 50 fs, and all production runs were carried out in the constant NVE ensemble for 1 ns. Each MS-EVB simulation used a time step of 0.5 fs with a long-range cutoff of 9.0 Å and an Ewald summation with an error of 10^{-5}. In order to quantify the nuclear quantum effects (NQEs), additional thermostated ring polymer molecular dynamics[62] (TRPMD) of the MS-EVB 3.2 model were conducted by the i-PI force engine[63] coupled to LAMMPS. The ring polymer contraction[64] (RPC) and multiple time stepping (MTS) methods were employed. The centroid contraction was shown to be sufficiently accurate for hydrated excess protons[42] and was used herein for all TRPMD simulations. The MS-EVB methodology described earlier with three solvation shell searching was used to compute the forces on the path integral centroid, while the same MS-EVB settings but with two solvation shell state searching were used as the reference forces. The inner time step for the MTS integrator was 0.15 fs, while the outer time step was 1.2 fs. Ten independent runs were performed for 504 ps each initiated from independent samples in classical MS-EVB simulations.

In total, three EDS-AIMD(OO) simulations of 1 HCl in 128 water molecules with a box side length of 15.72 Å and two EDS-AIMD(OH) simulations of a H^+ in 128 water molecules with a box side length of 15.64 Å were equilibrated in the constant NVT ensemble using a Nose-Hoover chain thermostat with a time constant of 11.12 fs, followed by 80 and 200 ps in the constant NVE ensemble for EDS-AIMD(OO) and EDS-AIMD(OH), respectively. EDS parameters were identified from our previous work[49,53] for the BLYP exchange−correlation functional[65,66] with the D3 Grimme dispersion interaction.[67,68] All EDS-AIMD simulations were carried out with the Quickstep module in CP2K[69] and PLUMED[70,71] packages using Goedecker−Teter−Hutter (GTH) pseudopotentials[72] with a TZV2P basis set having a plane-wave cutoff of 400 Ry. The three EDS-AIMD(OO) runs had an average temperature of (1) 301 ± 10.3 K, (2) 290 ± 9.9 K, and (3) 292 ± 9.7 K, and the three EDS-

https://doi.org/10.1021/jacs.1c08552
J. Am. Chem. Soc. 2021, 143, 18672−18683

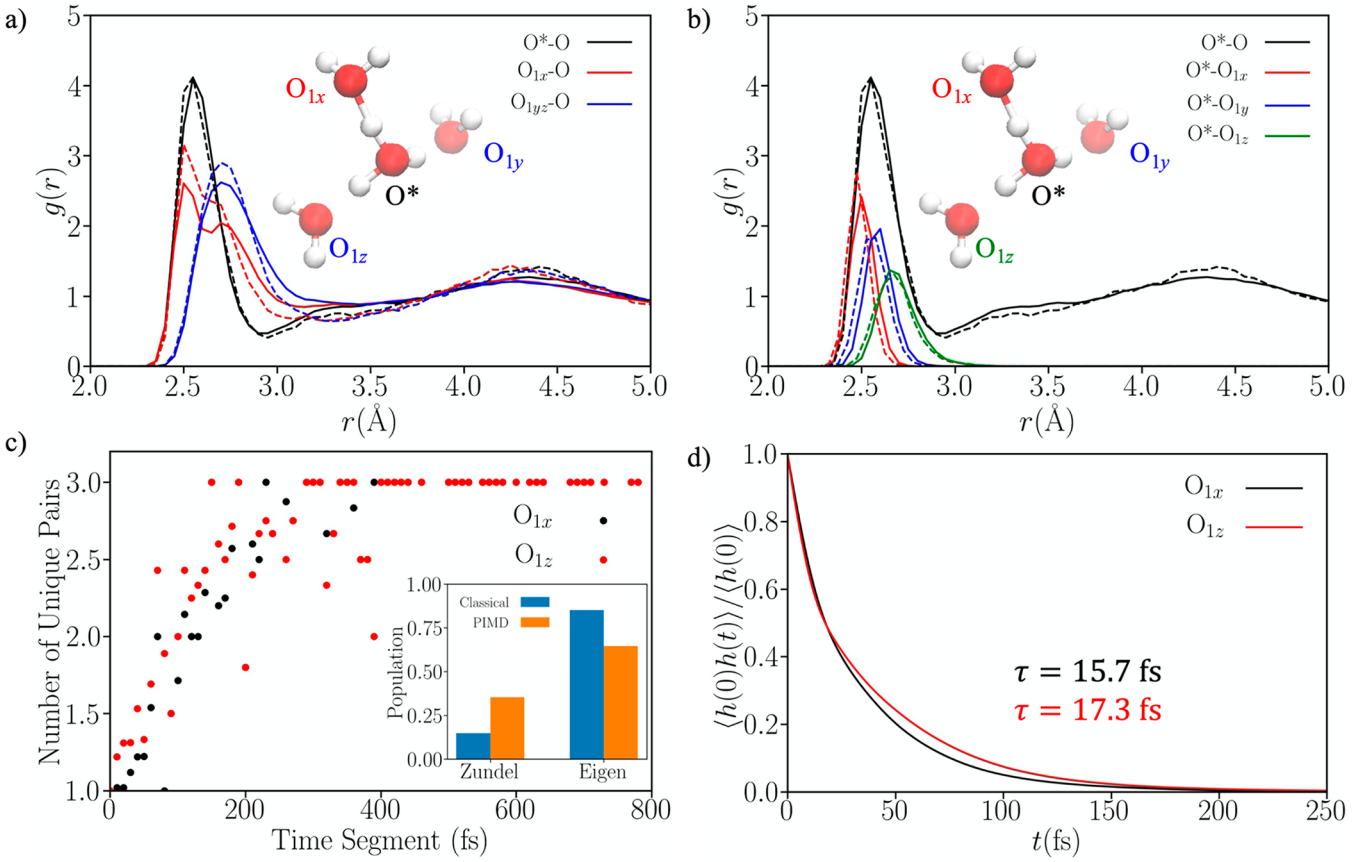

Figure 1. Solvation structure of the hydrated excess proton and the special pair dance dynamics. (a) O−O radial distribution functions of the O*−O (black), O_{1x}−O (red), and O_{1yz}−O (blue) in EDS-AIMD(OH) classical simulations (solid) and PIMD EDS-AIMD(OH) simulations (dashed) with NQEs. The O* is the oxygen with the most hydronium-like character (most probable), while O_{1x}, O_{1y}, and O_{1z} are the first solvation shell oxygens of H_3O^+ in the order of strongest to weakest hydrogen bond. (b) Classical (solid) and quantum (dashed) EDS-AIMD(OH) O*−O RDF (black) decomposed into three water molecules, O_{1x} (red), O_{1y} (blue), and O_{1z} (green). (c) Number of unique O_{1x} (black) and O_{1z} (red) identities in time segments where the proton does not hop, as a function of segment length. The inset shows the population of Zundel and Eigen, respectively (see Section S3 of the SI for details). (d) Continuous correlation function of the O_{1x} (black) and O_{1z} (red) of eq 4. The time constant was obtained from $\int dt\ C(t)$.

AIMD(OH) runs had an average temperature of (1) 293 ± 10.1 K, (2) 298 ± 10.2 K, and (3) 294 ± 10.1 K. In order to examine the NQEs on proton solvation thermodynamics, an additional path integral molecular dynamics (PIMD) was performed with EDS-AIMD(OH) in i-PI[63] coupled to CP2K. The PIMD was first equilibrated by a Langevin thermostat with a relaxation time of 15 fs started from the NVT equilibrated configuration of classical nuclei. The production PIMD was run after that for ∼32 ps with the Langevin relaxation time softened to 100 fs. A time step 0.5 fs was used to integrate the dynamics, and the full *ab initio* calculations were conducted on the total 30 path integral beads. For quantum dynamics of EDS-AIMD(OH), six independent TRPMD simulations were performed using the RPC and MTS approach for 200 ps per run. The reference potential was a machine learned (ML) potential trained with energies and forces sampled in the EDS-BLYP-D3(OH) NVT equilibration using the DeepMD-kit.[73] An inner time step of 0.5 fs and an outer time step of 2 fs was used to integrate the dynamics.

Instantaneous Normal Mode Analysis. Instantaneous normal mode (INM) calculations[74,75] were carried out to further compare structural vibrations and infrared absorption frequencies, with the goal of better clarifying the solvation structure of the hydrated excess proton. The INM calculations were derived as in a prior report,[34] but were augmented here by using both MS-EVB 3.2 and EDS-AIMD(OO) trajectories in a time-dependent fashion. The hydrated excess proton was identified as the proton in the hydronium cation with the lowest δ value; all water molecules within a 5 Å radius were included in the NMA calculation. Further NMA calculations restricted the number of water molecules to include only those in the second solvation shell, since this approach was shown to capture the extent of charge delocalization of the positive charge defect in the excess proton complex.[26] All NMA calculations were calculated using the B3LYP exchange−correlation functional[76] with a 6-311++G(p,d) basis set in the Gaussian 09 software package.[77] It should also be noted that each NMA was carried out in the absence of energy minimization, and so all imaginary frequencies were discarded prior to analysis.

RESULTS AND DISCUSSION

Solvation Structure of Hydrated Excess Proton. Figure 1a illustrates the solvation structure of the hydrated proton in EDS-AIMD(OH) simulations, while the results of other simulation methods provide similar conclusions (see Figure S3). The O−O RDFs include all oxygen atoms in the system, those centered on the most probable hydronium-like (O*, black), the special partner oxygen ($O_{1x,}$ red), and the remaining water molecules in the hydrated proton complex (O_{1yz}, blue). In these calculations, O_{1x}, O_{1y}, and O_{1z} are defined as the neighboring water molecules with increasing value of the proton sharing parameter, δ (defined as the difference between two O−H distances involving the shared proton, i.e., $r_{OH}-r_{O^*H}$) around the most probable hydronium.

We note that the solvation structures of the hydronium-like structure and the special partner oxygen are not identical, as

https://doi.org/10.1021/jacs.1c08552
J. Am. Chem. Soc. 2021, 143, 18672−18683

indicated by different O* and O_{1x} RDFs. In a symmetric Zundel cation, the excess proton would remain in the center of the two flanking water molecules, which would then make these flanking waters nearly identical. Even when the excess proton "rattling" is factored into this Zundel picture, the ensemble average of this rattling would still give rise to identical solvation environments of the two flanking water molecules and nearly identical solvation structures for the O* and O_{1x}. We also observed the O_{1x} becomes more similar to O* in Figure 1a after including the NQEs, but O* and O_{1x} still exhibit clearly distinct solvation structures. We also note that a recent study[40] has distinguished Zundel and Eigen cations differently from the present work, with a criterion that is based on the O*−O_{1x} distance being less than or greater than 2.7 Å, respectively, for Zundel and Eigen. This classification method is questionable, however, since we note that for the simulation methods reported here all O_{1x} distances were found to be less than 2.7 Å, so the criterion used in this other work would never identify a distorted Eigen cation as has been done here. A more Zundel-like cation picture also is at odds with the difference in the in O* and O_{1x} RDFs seen here with four different simulation approaches.

The calculated RDFs in this work indeed indicate a distinction between the hydronium-like structure having the excess proton (O*) and the special partner (O_{1x}), which is a clear characteristic of a distorted Eigen cation. (We note that the distorted Eigen cation has also been suggested as the most thermodynamically stable structure in recent AIMD studies which additionally used activated rate theory to characterize proton transfers in water.[78]) In a Zundel-like proton configuration picture,[79] one would see clear evidence of a single water molecule positioned closer to the hydronium-like cation, which is in agreement with the RDFs found in Figure 1a. However, these various static snapshots ignore the important dynamics of the protonated complex. If the Zundel-like picture also represented the actual dynamics of the system, the O*−O RDF would match the O_{1x} RDF, corresponding to a dominant first peak for the special partner and integrating to a coordination of a single water molecule. In contrast, the ensemble- and time-averaged structure shows a single peak in the O*−O RDF and an average coordination of approximately three water molecules. Given these findings—coupled with the preference for the excess proton to associate with one water molecule at a given instant—the present simulations strongly suggest that a distorted Eigen best characterizes the hydrated excess proton. By virtue of the distorted Eigen picture, we can also incorporate the special pair (i.e., instantaneous two-water shared proton picture), while additionally accounting for the dynamics of the hydrated excess proton involving other water molecules in the larger Eigen cation complex. In fact, the picture of a distorted Eigen cation as best representing the hydrated excess proton structure first emerged from simulation more than 20 years ago.[17]

Special Pair Dance Revisited. It has previously been shown that the hydrated excess proton is not a static complex, but is a very dynamic one. In prior work,[22] it was revealed that the identity of the hydrated proton's special partner switches with other waters in the hydrated complex on a short time scale of tens of femtoseconds. Here we revisit this result using the EDS-AIMD(OH) hydrated excess proton model, which is the most recent model and one we consider to be the most accurate (it includes the use of the highly accurate MB-pol model[54−57] as the EDS reference for the water solvent).

In Figure 1b we show more detail of the O*−O RDF of the EDS-AIMD(OH) model from Figure 1a. We further decompose the first peak into its special partner (O_{1x}) and two, less hydrogen-bonded water molecules (O_{1y} and O_{1z}). We again defined these water molecules with increasing δ value. When examining Figure 1b, three distinct peaks are found with varying distances from the most hydronium-like oxygen, which correspond with the closest water being the special partner. The overall statistically combined RDF peak (black line) is clearly unimodal. This result is another indication of the distorted Eigen cation as being the predominant hydrated proton species, where the three water molecules in the first shell are statistically unique when decomposed into three component peaks, and one water molecule on average is found to be closer to the hydronium core. However, this is an average over all configurations, and the specific water molecules contributing to these three peaks will vary with time.

We next investigate the dynamics of the closest and furthest water molecule in Figure 1c and d. We begin by examining the number of unique O_{1x} and O_{1z} identities for periods of time where the most hydronium-like oxygen does not change, i.e., no proton hopping (Figure 1c). For short times, there is only one unique water molecule for the special partner and the third furthest water molecule. As the length of time in which the proton resides on a single water molecule increases, the number of water molecules that could be identified as the special partner (O_{1x}) and the furthest water molecule (O_{1z}) increases to 3. These findings indicate that when the proton resides on a single water molecule for short times—as is the case for single configuration snapshots and proton rattling events—only one water molecule is found to be the special partner and another water molecule can be identified as O_{1z}. On the other hand, during long periods of no proton transfer events, the special partner and corresponding O_{1z} water molecules are dynamically switching in the first solvation shell of the H_3O^+ motif and thus point to the significance of accounting for all three water molecules in the proton complex instead of using static configurations, such as is often the case for Zundel-like configurations.

It is then important to check whether the Eigen-like or the Zundel-like species dominates the dynamics of the hydrated excess proton. As shown in the inset of Figure 1c, the Eigen dynamics (see Section S3 of the SI for detailed definitions) is the most populated process in the EDS-AIMD(OH) simulations, while the NQEs increase the population of Zundel dynamics, the NQEs do not change the overall dominance of the distorted Eigen cation. We note that although EDS-AIMD(OH) improves BLYP-D3-level DFT significantly to a comparable accuracy with CCSD(T) for the gas-phase PT barriers (Figure S2 of the SI), EDS-AIMD(OH) still slightly underestimates this PT barrier. This means that the Zundel population is likely somewhat overestimated in the EDS-BLYP-D3(OH) AIMD simulations, as well as when NQEs are included with PIMD. The relative dominance of the distorted Eigen cation, as found from this dynamical analysis, is consistent with the result of the solvation structure analysis shown in Figure 1a.

We additionally calculated the continuous correlation function in Figure 1d for the special partner and the O_{1z} water molecule according to the following equation:

https://doi.org/10.1021/jacs.1c08552
J. Am. Chem. Soc. 2021, 143, 18672−18683

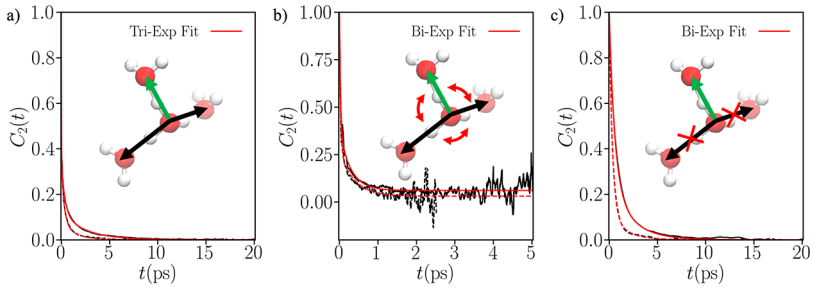

Figure 2. Anisotropy plots using eq 5 for the O*−O unit vector. The anisotropy plots are broken down based on (a) total anisotropy, (b) special pair dance (no proton transfer), and (c) long-lived special pair (no special pair dance). The solid curves represent the classical MS-EVB results, while the dashed curves represent the quantum MS-EVB results. The same plots in log scale can be found in Figure S6.

Table 1. Proton Anisotropy Decay (Eq 5) Time Scales and Amplitudes

system	a_1	τ_1 (fs)	a_2	τ_2 (ps)	a_3	τ_3 (ps)	C
MS-EVB[a]	0.65	12	0.23	0.36	0.12	2.5	0.00
aMS-EVB[a]	0.66	10	0.23	0.32	0.11	2.3	0.00
EDS-AIMD(OO)[a]	0.74	17	0.17	0.49	0.09	3.2	−0.01
EDS-AIMD(OH)[a]	0.74	17	0.19	0.38	0.08	2.6	0.00
EDS-AIMD(OH) TRPMD	0.49	12	0.36	0.083	0.15	1.4	0.00
MS-EVB TRPMD	0.63	15	0.29	0.27	0.08	1.4	0.00
experiment[b]				∼0.2[c]		∼1.5[d]	

[a]Nuclei are treated classically. [b]Experimental data from ref 39. [c]The time scale (referred to as "fast component" in ref 39) shows a weak dependency on concentration. The 1 M experimental data are used here. [d]The data for 1 M, 2 M, and 4 M (referred to as "slow component" in ref 39) are used to extrapolate to the MS-EVB simulation concentration of 0.22 M. The details of the extrapolation can be found in Section S6 of the SI.

$$C(t) = \frac{\langle h(0)\, h(t)\rangle}{\langle h(0)\rangle} \tag{4}$$

where $h(t) = 1$ during segments of the trajectory where the O_{1x} or O_{1z} does not change and 0 for all other times. This is similar to the continuous correlation function used for the excess proton structure.[80] We find that the continuous correlation functions for both the O_{1x} and O_{1z} are very similar. By integrating these correlation functions, we can gain an estimate of the lifetime of these species in the distorted Eigen cation, and we find a lifetime of 15.7 and 17.3 fs for O_{1x} and O_{1z}, respectively. These again point to the dynamical nature of the surrounding water molecules in the distorted Eigen cation, with the special partner continuously evolving between the hydronium core and several (three) water molecules dynamically solvating it, with excess proton rattling events occurring between all of these three waters but at different times.

Special Pair Anisotropy Decay. It is critically important to make contact with experimental data and to reinterpret it if necessary. In this vein, recent nonlinear infrared spectroscopy data from Carpenter et al.[38] indicate that the reorientation of the hydrated excess proton complex features two measurable time scales of ∼2 ps and ∼200 fs, which was obtained by measuring the intensity via parallel and perpendicular pulses at 1740−1790 cm^{-1}. In this important new experimental work, the vibrational bending of the flanking water molecules in the special pair was assigned to 1750 cm^{-1}. These authors also de-emphasized certain phenomena—notably, the complete reorientation of the hydrated excess proton complex without proton transfer, rapid structural fluctuations, and energy and thermal transfer from the hydrated complex to surrounding aqueous environment—as possible structural reorientations that might explain the ∼2 ps time scale. Instead, they suggested that the long reorientation time scale corresponds to irreversible proton transfer. Additionally, they suggest that the special pair dance could not play a role in their results, as one might have expected a change in the identity of the special partner to reorient the transition dipole more rapidly than either the ∼2 ps or ∼200 fs time scale. Since the special pair dance phenomenon is uniquely associated with the distorted Eigen species, these time scales were used as evidence by Carpenter et al. to advocate a more distorted Zundel-like picture.[37]

Here, we seek to understand through our simulation data the structural reorientations of the hydrated excess proton complex that correspond to the observed experimental anisotropy time scales, with special emphasis on elucidating the nature of the special pair dynamics and irreversible proton transport. It is very common in MD simulations of water to calculate the anisotropy of the O−H stretch by using the unit vector along the O−H bond.[81] Given recent findings using a two-water or special pair approach, we decided to define the unit vector along the O*−O axis of the special pair. Anisotropy calculations were then determined using the second Legendre polynomial ($P_2(x) = (3x^2 - 1)/2$) of the unit vector defining the special pair, such that

$$C_2(t) = \frac{\langle P_2(\hat{\boldsymbol{u}}(0)\, \hat{\boldsymbol{u}}(t))\rangle}{\langle P_2(\hat{\boldsymbol{u}}(0)\, \hat{\boldsymbol{u}}(0))\rangle} \tag{5}$$

Here, the $\langle\cdots\rangle$ denotes an ensemble average of the unit vector.

Figure 2a illustrates the anisotropy decay of the O*−O special pair from classical and quantum MS-EVB 3.2 simulations with the special pair defined as the O*−O that has the lowest δ parameter (corresponding O*−O anisotropy plots for classical aMS-EVB, EDS-AIMD(OO), and EDS-AIMD(OH) can be found in Section S5 of the SI). By fitting a triple-exponential function (eq S1) to the total anisotropy

https://doi.org/10.1021/jacs.1c08552
J. Am. Chem. Soc. 2021, 143, 18672−18683

decay (see Discussion in Section S6 of the SI) from MS-EVB classical simulations, we obtained time constants of 12 fs, 0.36 ps, and 2.5 ps, with corresponding exponential term amplitudes of 0.65, 0.23, and 0.12. Comparable values were obtained from the other simulation methods, as indicated in Table 1. Of particular importance is that these time constants and amplitude data can be replicated across various simulation methods, confirming that our findings are not unique to the MS-EVB simulations. It is worth noting that, with quantized nuclei, the time constants τ_2 and τ_3 of MS-EVB TRPMD are in good agreement with the time constants determined from 2D-IR experiments,[38,39] while an additional fast time scale τ_1 with a non-negligible amplitude is seen herein from our simulations. It was also found in EDS-AIMD(OH) simulations that NQEs reduce the time constants τ_2 and τ_3, resulting in an overcorrected τ_2 but bringing the long-lived time scale τ_3 into better agreement with the experimental value. To identify the precise structural phenomena corresponding to these time constants, we then removed specific structural dynamics from the trajectory input for the anisotropy decay calculations (how we achieved the removal is discussed below) and refit that data to a biexponential function. Since we observed good agreement between the MS-EVB and EDS-AIMD simulations, we conducted subsequent calculations using only the more computationally efficient MS-EVB approach, as it can be run much longer and thus provide better statistics in comparison to the EDS-AIMD approach.

First, we removed from the anisotropy calculation any contribution in the trajectory that was associated with proton transfer, but kept other phenomena intact, including the special pair dance. As noted earlier, this is a process wherein the identity of the special partner changes in a distorted Eigen cation, but with the absence of any change in the identity of the central hydronium-like core. We parsed the trajectory into segments where the excess proton remained on a single water molecule and next calculated the unit vector for the special pair. The anisotropy was then calculated for each of these no-proton-transfer segments and averaged over all of them. The special pair dance anisotropy calculation is shown in Figure 2b for MS-EVB 3.2; as indicated therein, we obtained time constants of 28 fs and 0.29 ps from classical simulations and 27 fs and 0.38 ps from quantum simulations (Table 2).

Table 2. Anisotropy Decay without Proton Hopping

system	a_1	τ_1 (fs)	a_2	τ_2 (ps)	C
MS-EVB	0.68	28	0.32	0.29	0.06
aMS-EVB	0.70	29	0.30	0.31	0.05
MS-EVB TRPMD	0.76	27	0.24	0.38	0.03
MS-EVB TRPMD[a]	0.68	15	0.32	0.27	0.00

[a]Taken from Table 1 of total anisotropy. The amplitudes a_1 and a_2 are renormalized to unitary for better comparison.

Comparing to time constants listed in Table 1, we found that the long time scale τ_3 vanishes while the τ_1 and τ_2 are retained. Since the proton transfer is eliminated from the anisotropy calculation here, we identified the fading time scale τ_3 as corresponding to the special pair vector reorientation associated with proton transfers. Previous MS-EVB simulations have shown that the identity of the special pair interchanges on tens of fs time scales,[28] which is consistent with the 28 fs identified in this anisotropy calculation. This rapid time scale is too fast to be resolved by current experimental techniques; in fact, it is faster than the shortest pulse used experimentally.

In a similar manner, we examined the slower time constant by removing the special pair dance from the total anisotropy calculations. Using this approach, we no longer define the special pair as the O*−O pair with the lowest δ value, but rather as the O−O vector between the hydronium oxygen and the water oxygen to which the excess proton hops. For example, if at time step 0 the hydronium oxygen is molecule A and at time step t the hydronium oxygen is molecule B, then the special pair unit vector from time step 0 to time step t is defined as the O_A-O_B unit vector. This mimics a laser pulse with a finite time window longer than the special pair dance time scale resolves the special pair in a time-averaged manner. The anisotropy calculations for MS-EVB 3.2 are found in Figure 2c, and amplitude and time constant data are provided in Table 3. Note that for MS-EVB 3.2 we identified time constants of 0.56 and 2.17 ps from classical simulations and 0.32 and 1.58 ps from quantum simulations, revealing that the τ_1 listed in Table 1 vanishes in this analysis. It should also be pointed out that in all three tables there is seen an intermediate time scale τ_2 of sub-picosecond, which is comparable to one of the reorientation time scales discovered in pure water (Section S7 of the SI). We did not specifically analyze this motion, but since it involves the decay of an angular correlation, we presume it reflects the diffusive rotation of the overall Eigen complex.

Table 3. Anisotropy Decay without Special Pair Dance

system	a_2	τ_2 (ps)	a_3	τ_3 (ps)	C
MS-EVB	0.74	0.56	0.26	2.2	0.00
aMS-EVB	0.67	0.53	0.33	1.8	0.00
MS-EVB TRPMD	0.88	0.32	0.12	1.6	0.00
MS-EVB TRPMD[a]	0.78	0.27	0.22	1.4	0.00

[a]Taken from Table 1 of total anisotropy. The amplitudes a_2 and a_3 are renormalized to unitary for better comparison.

It must be appreciated that we were able to analyze these anisotropy plots while fully retaining the distorted Eigen cation picture of the hydrated excess proton complex. By removing the special pair dance from the distorted Eigen cation we were able to recover the long-lived time constant; analogously, by removing the proton transport component we were able to retain the special pair dance. In addition to confirming the agreement between the time constants and amplitudes between the biexponential fits to the total triexponential fits, these findings indicate that (a) the fast time constant correlates to the special pair dance and (b) the slow time constant corresponds to irreversible proton transfer. These hypotheses are supported by good agreement with the time scales and physical processes obtained from recent 2D-IR experiments. Moreover, all of this agreement is obtained without having to do away with the distorted Eigen cation picture.

Instantaneous Normal Mode Analysis. Our simulation methods show good agreement with the anisotropy time scales determined experimentally. However, the issue of the experimental evidence for the special pair dance also prompted an investigation reported herein of the correspondence between the special pair dance and specific vibrational frequencies. With this process depicted as a series of dynamic switches between the hydrated excess proton special pair, we utilized configurations within a 100 fs time span from the MS-

https://doi.org/10.1021/jacs.1c08552
J. Am. Chem. Soc. 2021, 143, 18672−18683

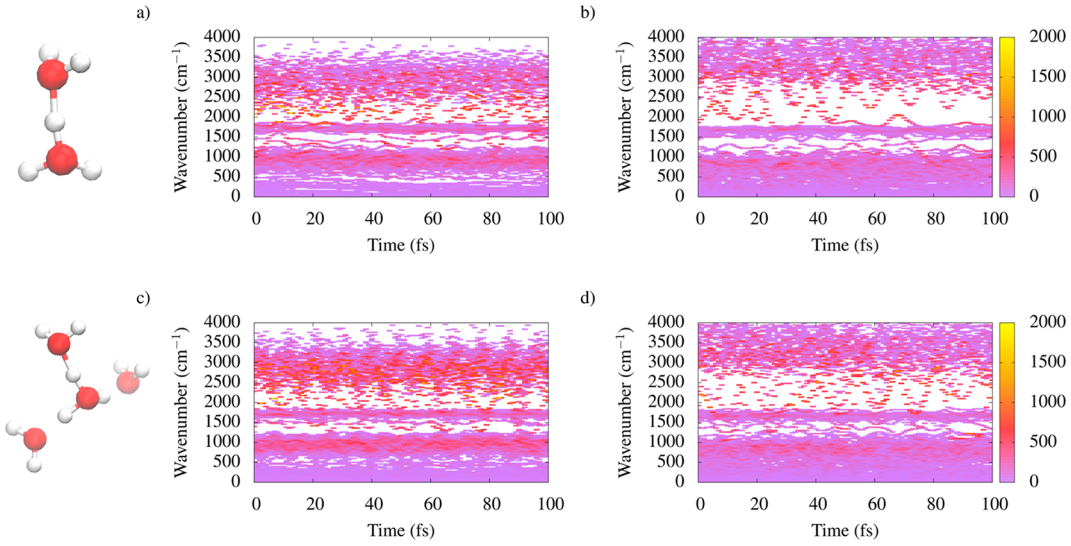

Figure 3. Spectral density as a function of time for Zundel (a and b) and Eigen (c and d) configurations using configurations taken from MS-EVB 3.2 (a and c) and EDS-AIMD (b and d). Zundel and Eigen are defined based on having 1 (Zundel) or 3 (Eigen) unique special pair water molecules during the 100 fs segment.

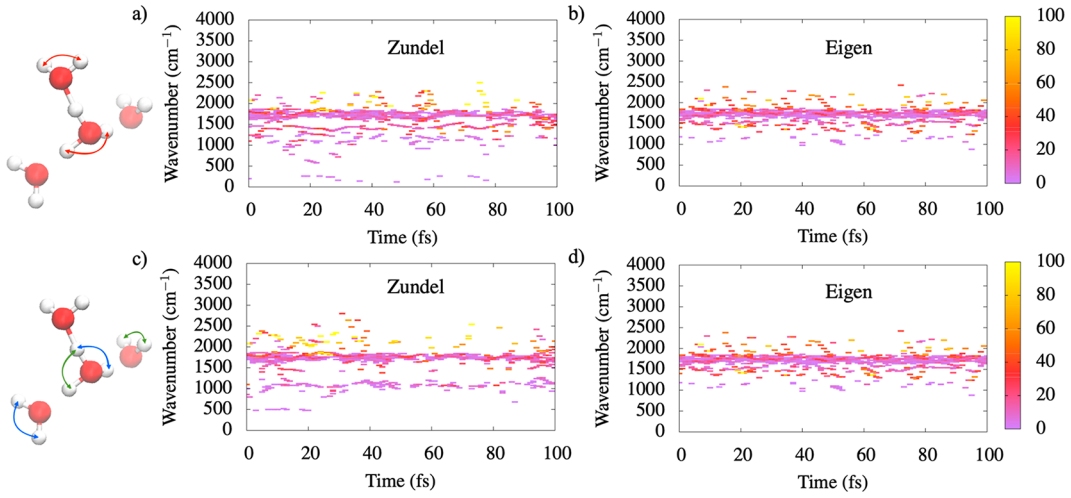

Figure 4. Spectral density as a function of time for H−O−H bends in a Zundel (a and c) period and an Eigen (b and d) period using data obtained from MS-EVB 3.2 simulations. Panels a and b show the spectral density for normalized normal modes whose H−O−H bends >5° in the special pair, while panels c and d show the spectral density of H−O−H bends >5° in other O*−O pairs.

EVB and EDS-AIMD(OO) results that correspond to the special pair dance. Instantaneous normal mode analysis was then applied to configurations separated by 1 fs, which differs from prior gas-phase NMA calculations that pick randomly selected configurations; accordingly, our method enables us to observe the time evolution of the normal modes. We note that the normal mode approach sacrifices some accuracy by not taking anharmonicity into account,[82,83] but it enables us to correlate instantaneous frequencies on a B3LYP level of the potential energy surface to specific molecular motions for given configurations, and moreover the approach has exhibited accuracy by reproducing the 1750 cm^{-1} band of particular interest in ref 34.

Two 100 fs segments obtained from MS-EVB 3.2 and EDS-AIMD(OO) simulations were selected where the hydronium-like molecular index remained unchanged. In the first segment, the identity of the special partner changed between the three water molecules; in contrast, the identity of the special pair remained unchanged in the second segment. We defined the first 100 fs segment as "Eigen" due to the observed special pair dance dynamics and the second as "Zundel" due to the static excess proton shared by two waters during the time period. We note that static Zundel-like geometries are not uncommon in an Eigen period due to the rattling of the excess proton shared between O* and the special partner, and thus frequency analysis based on static and geometric criteria in previous studies[34,52,83] may assign a portion of Eigen signals as Zundel. All waters and hydronium molecules whose oxygen atoms were found to reside within a 5 Å radial cutoff of the excess proton were included in the INM calculations, while another water selection strategy using second solvation shell water can be found in Section S8 of the SI.

Figure 3 shows the spectral density of the normal modes as a function of time, with configurations pulled from MS-EVB 3.2 and EDS-AIMD(OO) trajectories. Upon first inspection, we see many similarities in the spectral density plots, independent of the simulation method and whether the 100 fs segments were defined as Eigen or Zundel. The most striking difference

https://doi.org/10.1021/jacs.1c08552
J. Am. Chem. Soc. 2021, 143, 18672−18683

is the mean distribution of the OH stretches obtained from MS-EVB and EDS-AIMD(OO) simulations, that MS-EVB sampled configurations have the OH stretching band at around 3000 cm^{-1} while the EDS-AIMD(OO) shows the stretching band at around 3500 cm^{-1}. Of special interest is the frequency range around 1750 cm^{-1}, since this corresponds to the special pair flanking water bend. As indicated in Figure 4, there is a persistent spectroscopic signature at this frequency for both Zundel and Eigen periods, and it is not found only within a Zundel complex.

We next selected normal modes (illustrated by the molecular figures in Figure 4 and described below as well as in the figure caption) from these calculations that exhibited flanking water bending within the Zundel trajectory (Figure 4a,c) and Eigen trajectory (Figure 4b,d) from MS-EVB trajectories, while the analysis on EDS-AIMD(OO) trajectories gives similar results (see Section S9 of the SI). If flanking H−O−H angles in the special pair (Figure 4a,c) or other O*−O pairs in the first solvation shell (Figure 4b,d) changed by more than 5 degrees in a normalized normal mode, the mode was pulled and the spectral density of these modes was normalized by the number of them and plotted. In both the Zundel and Eigen trajectories, H−O−H bending could be found at 1750 cm^{-1} that did not result only from the special pair but rather from other O*−O pairs in the $H_9O_4^+$ motif. This finding confirms that the 1750 cm^{-1} resonance is independent of the structure classification, which is in good agreement with prior work indicating that vibrations at 1750 cm^{-1} can delocalize across 5−20 atoms.[34] This outcome may also explain why the experimentally obtained data could not confirm the special pair dance, in that many H−O−H bending vibrations can be excited instead of only the special pair itself.

CONCLUSIONS

In this work, we have utilized extensive simulations to further explore the structure of the hydrated excess proton, in the light of recent spectroscopic experiments. As such, we have obtained anisotropy decay data that closely match those obtained via nonlinear spectroscopy. By decomposing the anisotropy based on structural phenomena, we are able to identify anisotropy time scales that give rise to the special pair dance and the long-time decay of irreversible proton transfer. The processes associated with these time scales agree with previous theoretical studies of the hydrated excess proton,[21,22] while also replicating the long-lived anisotropy decay achieved experimentally.[38] Perhaps most importantly, all of these results were obtained from several simulation methods that show the distorted Eigen cation, continuously undergoing a special pair dance, as the dominant "core" hydrated proton structure in the studied acid solutions. These findings also provide a consistent interpretation of the recent nonlinear spectroscopic observations but do not lend support to a distorted Zundel cation picture.[37−39,84]

By examining the spectroscopic signatures of the protonated complex within Eigen and Zundel cations from the simulation data and INM analysis, we observed, in both Eigen and Zundel structural periods, a persistent 1750 cm^{-1} signal arisen from flanking water bending for all three hydrogen-bonded pairs of H_3O^+, but not limited to just the special pair. This degeneracy, as well as the extremely fast dynamics of the special pair dance, introduces challenges in the interpretation of 2D-IR experimental measurements having finite time-width laser pulses. At the same time, we emphasize that selecting static structures from MD simulations and inferring spectroscopic information from them can be problematic without examining the actual dynamics. Moreover, an even simpler interpretation based on a one-dimensional effective potential picture (e.g., a symmetric or distorted Zundel cation inferred from a simple symmetric or asymmetric double-well picture) is not able to capture the actual hydrated proton structure and dynamics.

Experimental anisotropy decay data for the flanking water bend show that increasing the chloride concentration decreases the proton transfer rate, while Arrhenius plots of the anisotropy time scales indicate that increasing the chloride concentration lowers the activation energy of irreversible proton transport.[39] Transition state theory arguments were used to suggest that additional chloride ions, rather than excess protons, create entropic barriers to irreversible proton transport. Similarly, recent theoretical work[78] has also shown a concentration dependence of the O*−Cl ion pairing and proton transfer rate using transition state theory and Marcus theory, while also finding the distorted Eigen cation as the thermodynamically most stable state and the Zundel cation as a reaction intermediate. However, this latter work did not address the existence of an entropy barrier to proton transport. By contrast, our very recent analysis[41] has provided an atomistic-level explanation for these phenomena by examining the influence of temperature and concentration on excess proton structure and transport in concentrated HCl solutions. This latter effort has also further reinforced the conclusions reached in the present study.

ASSOCIATED CONTENT

Supporting Information

The Supporting Information is available free of charge at https://pubs.acs.org/doi/10.1021/jacs.1c08552.

Information regarding methodology and accuracy evaluation of EDS-BLYP-D3(OH); RDFs of MS-EVB 3.2, aMS-EVB 3.2, and EDS-AIMD(OO); classification scheme of Eigen and Zundel cations; anisotropy decay plots for MS-EVB 3.2 on a log scale; anisotropy decays for aMS-EVB 3.2 and EDS-AIMD; justification for anisotropy fitting method; normal mode analysis using second solvation shell; and spectral density of flanking water bend on EDS-AIMD trajectories (PDF)

AUTHOR INFORMATION

Corresponding Author

Gregory A. Voth − *Department of Chemistry, Chicago Center for Theoretical Chemistry, James Franck Institute, and Institute for Biophysical Dynamics, The University of Chicago, Chicago, Illinois 60637, United States;* orcid.org/0000-0002-3267-6748; Email: gavoth@uchicago.edu

Authors

Paul B. Calio − *Department of Chemistry, Chicago Center for Theoretical Chemistry, James Franck Institute, and Institute for Biophysical Dynamics, The University of Chicago, Chicago, Illinois 60637, United States;* orcid.org/0000-0001-8385-2628

Chenghan Li − *Department of Chemistry, Chicago Center for Theoretical Chemistry, James Franck Institute, and Institute for Biophysical Dynamics, The University of Chicago, Chicago, Illinois 60637, United States*

Complete contact information is available at: https://pubs.acs.org/10.1021/jacs.1c08552

Author Contributions

†P.B.C. and C.L. contributed equally to this work.

Notes

The authors declare no competing financial interest.

■ ACKNOWLEDGMENTS

This research was supported by the U.S. Department of Energy, Office of Basic Energy Sciences, Separation Science Program of the Division of Chemical Sciences, Geosciences, and Biosciences, under Award Number DE-SC0018648. The computational resources for this research were in part provided by the University of Chicago Research Computing Center (RCC) and in part from a computational grant from the U.S. Department of Defense (DOD) High Performance Computing Modernization Program at the Navy DOD Supercomputing Resource Centers.

■ REFERENCES

(1) Wraight, C. A. Chance and design—Proton transfer in water, channels and bioenergetic proteins. *Biochim. Biophys. Acta, Bioenerg.* **2006**, *1757*, 886−912.
(2) Decoursey, T. E. Voltage-Gated Proton Channels and Other Proton Transfer Pathways. *Physiol. Rev.* **2003**, *83*, 475−579.
(3) Cukierman, S. Et tu, Grotthuss! and other unfinished stories. *Biochim. Biophys. Acta, Bioenerg.* **2006**, *1757*, 876−885.
(4) Swanson, J. M. J.; Maupin, C. M.; Chen, H.; Petersen, M. K.; Xu, J.; Wu, Y.; Voth, G. A. Proton Solvation and Transport in Aqueous and Biomolecular Systems: Insights from Computer Simulations. *J. Phys. Chem. B* **2007**, *111*, 4300−4314.
(5) Kreuer, K.-D.; Paddison, S. J.; Spohr, E.; Schuster, M. Transport in Proton Conductors for Fuel-Cell Applications: Simulations, Elementary Reactions, and Phenomenology. *Chem. Rev.* **2004**, *104*, 4637−4678.
(6) Savage, J.; Tse, Y.-L. S.; Voth, G. A. Proton Transport Mechanism of Perfluorosulfonic Acid Membranes. *J. Phys. Chem. C* **2014**, *118*, 17436−17445.
(7) Arntsen, C.; Savage, J.; Tse, Y. L. S.; Voth, G. A. Simulation of Proton Transport in Proton Exchange Membranes with Reactive Molecular Dynamics. *Fuel Cells* **2016**, *16*, 695−703.
(8) Bernal, J. D.; Fowler, R. H. A Theory of Water and Ionic Solution, with Particular Reference to Hydrogen and Hydroxyl Ions. *J. Chem. Phys.* **1933**, *1*, 515−548.
(9) Grotthuss, C. J. D. v. *Ann. Chim.* **1806**, *LVIII*, 54.
(10) Agmon, N. The Grotthuss mechanism. *Chem. Phys. Lett.* **1995**, *244*, 456−462.
(11) Eigen, M. Proton Transfer, Acid-Base Catalysis, and Enzymatic Hydrolysis. Part I: ELEMENTARY PROCESSES. *Angew. Chem., Int. Ed. Engl.* **1964**, *3*, 1−19.
(12) Zundel, G.; Metzger, H. Energiebänder der tunnelnden Überschuß-Protonen in flüssigen Säuren. Eine IR-spektroskopische Untersuchung der Natur der Gruppierungen $H_5O_2^+$. *Z. Phys. Chem.* **1968**, *58*, 225.
(13) Knight, C.; Voth, G. A. The Curious Case of the Hydrated Proton. *Acc. Chem. Res.* **2012**, *45*, 101−109.
(14) Agmon, N.; Bakker, H. J.; Campen, R. K.; Henchman, R. H.; Pohl, P.; Roke, S.; Thämer, M.; Hassanali, A. Protons and Hydroxide Ions in Aqueous Systems. *Chem. Rev.* **2016**, *116*, 7642−7672.
(15) Tuckerman, M.; Laasonen, K.; Sprik, M.; Parrinello, M. Ab initio molecular dynamics simulation of the solvation and transport of hydronium and hydroxyl ions in water. *J. Chem. Phys.* **1995**, *103*, 150−161.
(16) Lobaugh, J.; Voth, G. A. The quantum dynamics of an excess proton in water. *J. Chem. Phys.* **1996**, *104*, 2056−2069.
(17) Schmitt, U. W.; Voth, G. A. The computer simulation of proton transport in water. *J. Chem. Phys.* **1999**, *111*, 9361−9381.
(18) Vuilleumier, R.; Borgis, D. An Extended Empirical Valence Bond Model for Describing Proton Mobility in Water. *Isr. J. Chem.* **1999**, *39*, 457−467.
(19) Marx, D.; Tuckerman, M. E.; Hutter, J.; Parrinello, M. The nature of the hydrated excess proton in water. *Nature* **1999**, *397*, 601−604.
(20) Marx, D. Proton Transfer 200 Years after von Grotthuss: Insights from Ab Initio Simulations. *ChemPhysChem* **2006**, *7*, 1848−1870.
(21) Lapid, H.; Agmon, N.; Petersen, M. K.; Voth, G. A. A bond-order analysis of the mechanism for hydrated proton mobility in liquid water. *J. Chem. Phys.* **2005**, *122*, 014506.
(22) Markovitch, O.; Chen, H.; Izvekov, S.; Paesani, F.; Voth, G. A.; Agmon, N. Special Pair Dance and Partner Selection: Elementary Steps in Proton Transport in Liquid Water. *J. Phys. Chem. B* **2008**, *112*, 9456−9466.
(23) Vuilleumier, R.; Borgis, D. Quantum Dynamics of an Excess Proton in Water Using an Extended Empirical Valence-Bond Hamiltonian. *J. Phys. Chem. B* **1998**, *102*, 4261−4264.
(24) Kornyshev, A. A.; Kuznetsov, A. M.; Spohr, E.; Ulstrup, J. Kinetics of Proton Transport in Water. *J. Phys. Chem. B* **2003**, *107*, 3351−3366.
(25) Tuckerman, M.; Laasonen, K.; Sprik, M.; Parrinello, M. Ab Initio Molecular Dynamics Simulation of the Solvation and Transport of H3O+ and OH- Ions in Water. *J. Phys. Chem.* **1995**, *99*, 5749−5752.
(26) Swanson, J. M. J.; Simons, J. Role of Charge Transfer in the Structure and Dynamics of the Hydrated Proton. *J. Phys. Chem. B* **2009**, *113*, 5149−5161.
(27) Asmis, K. R.; Pivonka, N. L.; Santambrogio, G.; Brümmer, M.; Kaposta, C.; Neumark, D. M.; Wöste, L. Gas-Phase Infrared Spectrum of the Protonated Water Dimer. *Science* **2003**, *299*, 1375.
(28) Headrick, J. M.; Diken, E. G.; Walters, R. S.; Hammer, N. I.; Christie, R. A.; Cui, J.; Myshakin, E. M.; Duncan, M. A.; Johnson, M. A.; Jordan, K. D. Spectral Signatures of Hydrated Proton Vibrations in Water Clusters. *Science* **2005**, *308*, 1765.
(29) Heine, N.; Fagiani, M. R.; Rossi, M.; Wende, T.; Berden, G.; Blum, V.; Asmis, K. R. Isomer-Selective Detection of Hydrogen-Bond Vibrations in the Protonated Water Hexamer. *J. Am. Chem. Soc.* **2013**, *135*, 8266−8273.
(30) Heine, N.; Fagiani, M. R.; Asmis, K. R. Disentangling the Contribution of Multiple Isomers to the Infrared Spectrum of the Protonated Water Heptamer. *J. Phys. Chem. Lett.* **2015**, *6*, 2298−2304.
(31) Giberti, F.; Hassanali, A. A.; Ceriotti, M.; Parrinello, M. The Role of Quantum Effects on Structural and Electronic Fluctuations in Neat and Charged Water. *J. Phys. Chem. B* **2014**, *118*, 13226−13235.
(32) Kim, J.; Schmitt, U. W.; Gruetzmacher, J. A.; Voth, G. A.; Scherer, N. E. The vibrational spectrum of the hydrated proton: Comparison of experiment, simulation, and normal mode analysis. *J. Chem. Phys.* **2002**, *116*, 737−746.
(33) Xu, J.; Zhang, Y.; Voth, G. A. Infrared Spectrum of the Hydrated Proton in Water. *J. Phys. Chem. Lett.* **2011**, *2*, 81−86.
(34) Biswas, R.; Carpenter, W.; Fournier, J. A.; Voth, G. A.; Tokmakoff, A. IR spectral assignments for the hydrated excess proton in liquid water. *J. Chem. Phys.* **2017**, *146*, 154507.
(35) Thämer, M.; De Marco, L.; Ramasesha, K.; Mandal, A.; Tokmakoff, A. Ultrafast 2D IR spectroscopy of the excess proton in liquid water. *Science* **2015**, *350*, 78.
(36) Dahms, F.; Fingerhut, B. P.; Nibbering, E. T. J.; Pines, E.; Elsaesser, T. Large-amplitude transfer motion of hydrated excess protons mapped by ultrafast 2D IR spectroscopy. *Science* **2017**, *357*, 491.
(37) Fournier, J. A.; Carpenter, W. B.; Lewis, N. H. C.; Tokmakoff, A. Broadband 2D IR spectroscopy reveals dominant asymmetric $H_5O_2^+$ proton hydration structures in acid solutions. *Nat. Chem.* **2018**, *10*, 932−937.

(38) Carpenter, W. B.; Fournier, J. A.; Lewis, N. H. C.; Tokmakoff, A. Picosecond Proton Transfer Kinetics in Water Revealed with Ultrafast IR Spectroscopy. *J. Phys. Chem. B* **2018**, *122*, 2792−2802.
(39) Carpenter, W. B.; Lewis, N. H. C.; Fournier, J. A.; Tokmakoff, A. Entropic barriers in the kinetics of aqueous proton transfer. *J. Chem. Phys.* **2019**, *151*, 034501.
(40) Kundu, A.; Dahms, F.; Fingerhut, B. P.; Nibbering, E. T. J.; Pines, E.; Elsaesser, T. Hydrated Excess Protons in Acetonitrile/Water Mixtures: Solvation Species and Ultrafast Proton Motions. *J. Phys. Chem. Lett.* **2019**, *10*, 2287−2294.
(41) Calio, P. B.; Li, C.; Voth, G. A. Molecular Origins of the Barriers to Proton Transport in Acidic Aqueous Solutions. *J. Phys. Chem. B* **2020**, *124*, 8868−8876.
(42) Napoli, J. A.; Marsalek, O.; Markland, T. E. Decoding the spectroscopic features and time scales of aqueous proton defects. *J. Chem. Phys.* **2018**, *148*, 222833.
(43) Schmitt, U. W.; Voth, G. A. Multistate Empirical Valence Bond Model for Proton Transport in Water. *J. Phys. Chem. B* **1998**, *102*, 5547−5551.
(44) Day, T. J. F.; Soudackov, A. V.; Čuma, M.; Schmitt, U. W.; Voth, G. A. A second generation multistate empirical valence bond model for proton transport in aqueous systems. *J. Chem. Phys.* **2002**, *117*, 5839−5849.
(45) Wu, Y.; Chen, H.; Wang, F.; Paesani, F.; Voth, G. A. An Improved Multistate Empirical Valence Bond Model for Aqueous Proton Solvation and Transport. *J. Phys. Chem. B* **2008**, *112*, 467−482.
(46) Park, K.; Lin, W.; Paesani, F. A Refined MS-EVB Model for Proton Transport in Aqueous Environments. *J. Phys. Chem. B* **2012**, *116*, 343−352.
(47) Biswas, R.; Tse, Y.-L. S.; Tokmakoff, A.; Voth, G. A. Role of Presolvation and Anharmonicity in Aqueous Phase Hydrated Proton Solvation and Transport. *J. Phys. Chem. B* **2016**, *120*, 1793−1804.
(48) White, A. D.; Voth, G. A. Efficient and Minimal Method to Bias Molecular Simulations with Experimental Data. *J. Chem. Theory Comput.* **2014**, *10*, 3023−3030.
(49) White, A. D.; Knight, C.; Hocky, G. M.; Voth, G. A. Communication: Improved ab initio molecular dynamics by minimally biasing with experimental data. *J. Chem. Phys.* **2017**, *146*, 041102.
(50) Tse, Y.-L. S.; Knight, C.; Voth, G. A. An analysis of hydrated proton diffusion in ab initio molecular dynamics. *J. Chem. Phys.* **2015**, *142*, 014104.
(51) Biswas, R.; Carpenter, W.; Voth, G. A.; Tokmakoff, A. Molecular modeling and assignment of IR spectra of the hydrated excess proton in isotopically dilute water. *J. Chem. Phys.* **2016**, *145*, 154504.
(52) Carpenter, W. B.; Yu, Q.; Hack, J. H.; Dereka, B.; Bowman, J. M.; Tokmakoff, A. Decoding the 2D IR spectrum of the aqueous proton with high-level VSCF/VCI calculations. *J. Chem. Phys.* **2020**, *153*, 124506.
(53) Calio, P. B.; Hocky, G. M.; Voth, G. A. Minimal Experimental Bias on the Hydrogen Bond Greatly Improves Ab Initio Molecular Dynamics Simulations of Water. *J. Chem. Theory Comput.* **2020**, *16*, 5675−5684.
(54) Babin, V.; Leforestier, C.; Paesani, F. Development of a "First Principles" Water Potential with Flexible Monomers: Dimer Potential Energy Surface, VRT Spectrum, and Second Virial Coefficient. *J. Chem. Theory Comput.* **2013**, *9*, 5395−5403.
(55) Babin, V.; Medders, G. R.; Paesani, F. Development of a "First Principles" Water Potential with Flexible Monomers. II: Trimer Potential Energy Surface, Third Virial Coefficient, and Small Clusters. *J. Chem. Theory Comput.* **2014**, *10*, 1599−1607.
(56) Medders, G. R.; Babin, V.; Paesani, F. Development of a "First-Principles" Water Potential with Flexible Monomers. III. Liquid Phase Properties. *J. Chem. Theory Comput.* **2014**, *10*, 2906−2910.
(57) Reddy, S. K.; Straight, S. C.; Bajaj, P.; Huy Pham, C.; Riera, M.; Moberg, D. R.; Morales, M. A.; Knight, C.; Götz, A. W.; Paesani, F. On the accuracy of the MB-pol many-body potential for water: Interaction energies, vibrational frequencies, and classical thermodynamic and dynamical properties from clusters to liquid water and ice. *J. Chem. Phys.* **2016**, *145*, 194504.
(58) Li, C.; Swanson, J. M. J. Understanding and Tracking the Excess Proton in Ab Initio Simulations; Insights from IR Spectra. *J. Phys. Chem. B* **2020**, *124*, 5696−5708.
(59) Li, C.; Voth, G. A. Using Constrained Density Functional Theory to Track Proton Transfers and to Sample Their Associated Free Energy Surface. *J. Chem. Theory Comput.* **2021**, *17*, 5759−5765.
(60) Plimpton, S. Fast Parallel Algorithms for Short-Range Molecular Dynamics. *J. Comput. Phys.* **1995**, *117*, 1−19.
(61) Wu, Y.; Tepper, H. L.; Voth, G. A. Flexible simple point-charge water model with improved liquid-state properties. *J. Chem. Phys.* **2006**, *124*, 024503.
(62) Rossi, M.; Ceriotti, M.; Manolopoulos, D. E. How to remove the spurious resonances from ring polymer molecular dynamics. *J. Chem. Phys.* **2014**, *140*, 234116.
(63) Kapil, V.; Rossi, M.; Marsalek, O.; Petraglia, R.; Litman, Y.; Spura, T.; Cheng, B.; Cuzzocrea, A.; Meißner, R. H.; Wilkins, D. M.; Helfrecht, B. A.; Juda, P.; Bienvenue, S. P.; Fang, W.; Kessler, J.; Poltavsky, I.; Vandenbrande, S.; Wieme, J.; Corminboeuf, C.; Kühne, T. D.; Manolopoulos, D. E.; Markland, T. E.; Richardson, J. O.; Tkatchenko, A.; Tribello, G. A.; Van Speybroeck, V.; Ceriotti, M. i-PI 2.0: A universal force engine for advanced molecular simulations. *Comput. Phys. Commun.* **2019**, *236*, 214−223.
(64) Markland, T. E.; Manolopoulos, D. E. An efficient ring polymer contraction scheme for imaginary time path integral simulations. *J. Chem. Phys.* **2008**, *129*, 024105.
(65) Becke, A. D. Density-functional exchange-energy approximation with correct asymptotic behavior. *Phys. Rev. A: At., Mol., Opt. Phys.* **1988**, *38*, 3098−3100.
(66) Lee, C.; Yang, W.; Parr, R. G. Development of the Colle-Salvetti correlation-energy formula into a functional of the electron density. *Phys. Rev. B: Condens. Matter Mater. Phys.* **1988**, *37*, 785−789.
(67) Grimme, S. Accurate description of van der Waals complexes by density functional theory including empirical corrections. *J. Comput. Chem.* **2004**, *25*, 1463−1473.
(68) Grimme, S.; Antony, J.; Ehrlich, S.; Krieg, H. A consistent and accurate ab initio parametrization of density functional dispersion correction (DFT-D) for the 94 elements H-Pu. *J. Chem. Phys.* **2010**, *132*, 154104.
(69) VandeVondele, J.; Krack, M.; Mohamed, F.; Parrinello, M.; Chassaing, T.; Hutter, J. Quickstep: Fast and accurate density functional calculations using a mixed Gaussian and plane waves approach. *Comput. Phys. Commun.* **2005**, *167*, 103−128.
(70) Bonomi, M.; Branduardi, D.; Bussi, G.; Camilloni, C.; Provasi, D.; Raiteri, P.; Donadio, D.; Marinelli, F.; Pietrucci, F.; Broglia, R. A.; Parrinello, M. PLUMED: A portable plugin for free-energy calculations with molecular dynamics. *Comput. Phys. Commun.* **2009**, *180*, 1961−1972.
(71) Tribello, G. A.; Bonomi, M.; Branduardi, D.; Camilloni, C.; Bussi, G. PLUMED 2: New feathers for an old bird. *Comput. Phys. Commun.* **2014**, *185*, 604−613.
(72) Goedecker, S.; Teter, M.; Hutter, J. Separable dual-space Gaussian pseudopotentials. *Phys. Rev. B: Condens. Matter Mater. Phys.* **1996**, *54*, 1703−1710.
(73) Wang, H.; Zhang, L.; Han, J.; Weinan, E. DeePMD-kit: A deep learning package for many-body potential energy representation and molecular dynamics. *Comput. Phys. Commun.* **2018**, *228*, 178−184.
(74) Buchner, M.; Ladanyi, B. M.; Stratt, R. M. The short-time dynamics of molecular liquids. Instantaneous-normal-mode theory. *J. Chem. Phys.* **1992**, *97*, 8522−8535.
(75) Keyes, T. Instantaneous Normal Mode Approach to Liquid State Dynamics. *J. Phys. Chem. A* **1997**, *101*, 2921−2930.
(76) Becke, A. D. Density-functional thermochemistry. III. The role of exact exchange. *J. Chem. Phys.* **1993**, *98*, 5648−5652.
(77) Frisch, M. J.; Trucks, G. W.; Schlegel, H. B.; Scuseria, G. E.; Robb, M. A.; Cheeseman, J. R.; Scalmani, G.; Barone, V.; Petersson, G. A.; Nakatsuji, H.; Li, X.; Caricato, M.; Marenich, A.; Bloino, J.;

https://doi.org/10.1021/jacs.1c08552
J. Am. Chem. Soc. 2021, 143, 18672−18683

Janesko, B. G.; Gomperts, R.; Mennucci, B.; Hratchian, H. P.; Ortiz, J. V.; Izmaylov, A. F.; Sonnenberg, J. L.; Williams-Young, D.; Ding, F.; Lipparini, F.; Egidi, F.; Goings, J.; Peng, B.; Petrone, A.; Henderson, T.; Ranasinghe, D.; Zakrzewski, V. G.; Gao, J.; Rega, N.; Zheng, G.; Liang, W.; Hada, M.; Ehara, M.; Toyota, K.; Fukuda, R.; Hasegawa, J.; Ishida, M.; Nakajima, T.; Honda, Y.; Kitao, O.; Nakai, H.; Vreven, T.; Throssell, K.; Montgomery, J. A., Jr.; Peralta, J. E.; Ogliaro, F.; Bearpark, M.; Heyd, J. J.; Brothers, E.; Kudin, K. N.; Staroverov, V. N.; Keith, T.; Kobayashi, R.; Normand, J.; Raghavachari, K.; Rendell, A.; Burant, J. C.; Iyengar, S. S.; Tomasi, J.; Cossi, M.; Millam, J. M.; Klene, M.; Adamo, C.; Cammi, R.; Ochterski, J. W.; Martin, R. L.; Morokuma, K.; Farkas, O.; Foresman, J. B.; Fox, D. J.*GAUSSIAN 09*, Revision D.01; Gaussian Inc., 2009.

(78) Roy, S.; Schenter, G. K.; Napoli, J. A.; Baer, M. D.; Markland, T. E.; Mundy, C. J. Resolving Heterogeneous Dynamics of Excess Protons in Aqueous Solution with Rate Theory. *J. Phys. Chem. B* **2020**, *124*, 5665−5675.

(79) Daly, C. A.; Streacker, L. M.; Sun, Y.; Pattenaude, S. R.; Hassanali, A. A.; Petersen, P. B.; Corcelli, S. A.; Ben-Amotz, D. Decomposition of the Experimental Raman and Infrared Spectra of Acidic Water into Proton, Special Pair, and Counterion Contributions. *J. Phys. Chem. Lett.* **2017**, *8*, 5246−5252.

(80) Berkelbach, T. C.; Lee, H.-S.; Tuckerman, M. E. Concerted Hydrogen-Bond Dynamics in the Transport Mechanism of the Hydrated Proton: A First-Principles Molecular Dynamics Study. *Phys. Rev. Lett.* **2009**, *103*, 238302.

(81) Laage, D.; Stirnemann, G.; Sterpone, F.; Rey, R.; Hynes, J. T. Reorientation and Allied Dynamics in Water and Aqueous Solutions. *Annu. Rev. Phys. Chem.* **2011**, *62*, 395−416.

(82) Barone, V.; Biczysko, M.; Bloino, J. Fully anharmonic IR and Raman spectra of medium-size molecular systems: accuracy and interpretation. *Phys. Chem. Chem. Phys.* **2014**, *16*, 1759−1787.

(83) Yu, Q.; Carpenter, W. B.; Lewis, N. H. C.; Tokmakoff, A.; Bowman, J. M. High-Level VSCF/VCI Calculations Decode the Vibrational Spectrum of the Aqueous Proton. *J. Phys. Chem. B* **2019**, *123*, 7214−7224.

(84) Thämer, M.; De Marco, L.; Ramasesha, K.; Mandal, A.; Tokmakoff, A. Ultrafast 2D IR spectroscopy of the excess proton in liquid water. *Science* **2015**, *350*, 78−82.

https://doi.org/10.1021/jacs.1c08552
J. Am. Chem. Soc. 2021, 143, 18672−18683